Adaptive Spectral Carriers: Time Ordering, Reciprocal Memory, and Linked Coherent–Dissipative Response

Jeremy Rodgers

Reserved DOI: 10.5281/zenodo.23924603

everythingequation.com

3 November 2026

Abstract

A positive spectral carrier can evolve through the same physical variables whose response it organizes. We construct a finite complex-amplitude network with reciprocal real memory from one coercive energy and declared dissipative and reactive mobilities. The coupled source has global solutions, an exact energy balance, exponential amplitude decay and memory relaxation. Along each realized memory history, the conditional amplitude evolution retains instantaneous coherent–dissipative alignment, but generally loses the fixed-carrier factorization. An exact interaction picture and a gap-free double-integral commutator estimate quantify that failure; ordered pulses and a moving but commuting symmetry control separate time ordering from carrier motion alone. The full feedback tangent contains additional amplitude–memory couplings and a causal kernel, and an exact example shows transient tangent expansion despite positive partial amplitude curvature. A changing metric contributes a further connection term. We derive a calibrated operator-response test, with explicit extrapolation, noise and mobility-calibration bounds, that distinguishes the linked law from an alternative preserving coherent eigenvalues while rotating eigenvectors. Independent numerical formulations, exact fixtures and reproducible synthetic calculations verify the stated finite realizations. The resulting extension of the Canonical Spectral-Curvature Field specifies when linked responses survive adaptation and what observations can test them, without inferring a common microscopic law from cross-domain spectral recurrence.

Contents

1 From a fixed carrier to an adaptive source **3**
- 1.1 Relationship to the previous programme . . . 3
- 1.2 Source state and observable contracts . . . 4
- 1.3 Conventions . . . 4

2 A reciprocal adaptive carrier from one energy **4**
- 2.1 Units and physical assumptions . . . 5
- 2.2 Instantaneous CSCF realization . . . 6

3 Conditional evolution and time ordering **6**
- 3.1 Two pulses and asymptotic sharpness . . . 8
- 3.2 A moving but commuting control . . . 8

4 Full feedback, memory and changing coordinates **8**
- 4.1 Exact transient expansion despite partial positivity . . . 9
- 4.2 The connection for a changing mobility metric . . . 10
- 4.3 Why the autonomous closure certificate changes . . . 10

5 A calibrated test of linked operator response **11**
- 5.1 Short-time reconstruction and a controlled remainder . . . 11
- 5.2 Preparation, metric and access . . . 13

6 Executed finite calculations **13**
- 6.1 Feedback trajectory and independent formulation . . . 13
- 6.2 Pulse ordering and the symmetric control . . . 15
- 6.3 Response reconstruction and exact fixtures . . . 16
- 6.4 Public verification and evidence classes . . . 16

7 Consequences and focused extensions **17**
- 7.1 Physical implementation and driven organization . . . 17
- 7.2 Continuum domains and renormalization . . . 18

8 Conclusion **18**

1 From a fixed carrier to an adaptive source

The Canonical Spectral-Curvature Field (CSCF) organizes dissipative and coherent responses through a positive selfadjoint carrier and a declared real spectral symbol [1]. For a fixed finite carrier $K_d \geq 0$ and coherent generator $C = h(K_d)$, attenuation and phase evolution share spectral projections. Their combined response factors because the generators commute. When the carrier changes in response to its own amplitudes, the instantaneous spectral statement remains meaningful, but its relation to finite-time response requires a new argument.

The question addressed here is precise: under what stated conditions does a self-consistently evolving carrier support linked coherent and dissipative dynamics, how does time ordering modify that linkage, and which observable responses distinguish it? Three distinctions determine the answer. A realized memory history defines a conditional amplitude equation, while a physical perturbation of the complete source also changes memory. Commutation at one instant differs from commutation across instants. Finally, eigenvalue lists retain less information than phase-sensitive operator response in calibrated coordinates.

We construct an adaptive realization in which all three distinctions can be proved and tested. Positive edge stiffnesses depend exponentially on real memory coordinates. A single energy generates both the amplitude force and reciprocal memory feedback. Scalar dissipative and reactive mobilities align the instantaneous amplitude generators. This is a constitutive choice, motivated by the variational complex-amplitude structure familiar from the aligned complex Ginzburg–Landau setting [2]; it is specified here directly in finite dimension. The edge law, energy and mobilities are added physical hypotheses, rather than consequences of a pooled spectral profile.

The mathematical conclusions have a connected form. Energy coercivity supplies global well-posedness and uniform carrier bounds. Variation of constants gives an exact rotating-frame attenuation law and a bound on the error of the static factorization, without eigenvalue-gap assumptions. Differentiating the complete source gives the full feedback tangent; eliminating its memory block retains a causal kernel and an initial-memory term. These equations then specify the preparation resources needed for a paired-response test. The same operator residual that expresses the linked law has an explicit reconstruction error bound.

Nonautonomous evolution families and ordered exponential expansions are established tools [3, 4]. Projection and memory identities likewise belong to the established source-to-readout and response machinery [5]. The contribution here is the controlled adaptive realization and its linked source, propagation, feedback and observation results. All finite-dimensional proofs used to reach those conclusions are supplied below. No classification of arbitrary reversible–irreversible dynamics is intended.

1.1 Relationship to the previous programme

The CSCF paper develops the fixed-carrier functional calculus, physical mobility conversion, reciprocal storage and aligned complex-gradient realization [1]. *From Source Structure to Spectral Profiles* develops domain-specific generation mechanisms and information-retention limits for radial, spatial and outgoing-boundary constructions [6]. The spectral study records the cross-domain ratio evidence and its diagnostic limits [7]. Those reconstructions are background, not new results of this paper. In particular, no atomic bath, image-formation process or Kerr pole problem is identified with the adaptive network introduced here.

The new step is to let the carrier evolve through a declared source law while retaining an operational distinction between the two faces. The phrase *common carrier* concerns the relation between attenuation and phase within this realization. It does not assert that different physical domains possess the same matrix or microscopic interaction. Section 7 treats implementation, driving and continuum extensions.

1.2 Source state and observable contracts

Shadow Theory's source-to-readout architecture distinguishes source data from their retained records, and asks whether a proposed target is constant on readout fibres [5, 8]. Here the source state is $(z, m) \in \mathbb{C}^n \times \mathbb{R}^p$, together with fixed network, metric and mobility data. The evolving carrier is a function $K(m)$. An amplitude-only record retains z and omits m; a memory-resolved record retains both. Conditional operator probes additionally require the same memory history for all preparation columns.

This distinction has an immediate dynamical consequence. In the scalar special case $K(m) = 2/5 + e^m$, the source states $(z, m) = (1, 0)$ and $(1, \log 2)$ have the same amplitude readout but carrier values $7/5$ and $12/5$. Their amplitude velocities differ. Thus an autonomous amplitude-only first-order law cannot reproduce every source trajectory. This is an explicit failure of dynamical descent through the amplitude projection. Restricting preparations or retaining memory can change the target; neither operation follows merely from omitting a variable in notation.

1.3 Conventions

Vectors in $\mathbb{C}^n$ carry the standard inner product u^*v, linear in v. Matrix adjoints are denoted by *; real transposes by $^\top$. Unless subscripted F, norms are Euclidean vector norms or their induced operator norms. The Frobenius norm is $\|A\|_F^2 = \operatorname{tr}(A^*A)$. All differential equations are finite dimensional. We use the phase convention $z(t) \sim e^{-\mathrm{i}\omega t}$, so a positive reactive coefficient gives positive phase frequency. No stochastic noise is built into the source equations; measurement error is introduced separately.

2 A reciprocal adaptive carrier from one energy

Fix real vectors $b_e \in \mathbb{R}^n$, $1 \le e \le p$, and set $B_e = b_e b_e^\top$. For a network these are oriented incidence vectors, with $b_e^\top \mathbf{1} = 0$; the orientation does not affect B_e. Let $\mu, \kappa, \gamma, \eta > 0$ and $\alpha > 0$. Define

$$K(m) = \mu I + \sum_{e=1}^{p} e^{m_e} B_e, \tag{1}$$

$$F(z, m) = \frac{1}{2} z^* K(m) z + \frac{\kappa}{2} |m|^2 . \tag{2}$$

In dimensional formulas each edge stiffness is $k_e^0 e^{m_e}$ with $k_e^0 > 0$ in the same units as μ; the displayed equations and computations choose normalized $k_e^0 = 1$. Unequal fixed stiffnesses are also absorbed into b_e by multiplication by $\sqrt{k_e^0}$ once units are fixed.

Write $q = (\Re z, \Im z) \in \mathbb{R}^{2n}$ and

$$J = \begin{pmatrix} 0 & -I \\ I & 0 \end{pmatrix}, \qquad K_R = \operatorname{diag}(K, K), \qquad G = \gamma I + \alpha J. \tag{3}$$

The constitutive law uses dissipative mobility γI and skew mobility αJ on amplitudes, and dissipative mobility ηI on memory:

$$\dot{q} = -G \nabla_q F, \qquad \dot{m} = -\eta \nabla_m F. \tag{4}$$

Since $\nabla_q F = K_R q$ and $\partial_{m_e} F = \kappa m_e + e^{m_e} |b_e^\top z|^2/2$, the equations are

$$\dot{z} = -(\gamma + \mathrm{i}\alpha) K(m) z, \tag{5}$$

$$\dot{m}_e = -\eta \left(\kappa m_e + \frac{1}{2} e^{m_e} |b_e^\top z|^2 \right). \tag{6}$$

Both directions of the coupling come from the same F. Changing an amplitude contrast changes memory, while changing memory changes the edge stiffness. The skew term does no work on F. We use the real gradient convention, so no implicit factor from a Wirtinger derivative enters (5).

2.1 Units and physical assumptions

If z has amplitude units A and F has energy units E, then K and μ have units E/A^2, m is dimensionless, and κ has units E. Both γ and α have units $A^2/(E\,\mathrm{s})$, while η has units $1/(E\,\mathrm{s})$. Hence γK is an amplitude-decay generator and αK is an angular-frequency generator. Squared amplitude decays at twice the amplitude rate on a fixed mode.

Choose reference scales A_0, E_0, t_0 for numerical normalization. The dimensionless coefficients are $\widetilde{\mu} = \mu A_0^2/E_0$, $\widetilde{\gamma} = \gamma E_0 t_0/A_0^2$, $\widetilde{\alpha} = \alpha E_0 t_0/A_0^2$, $\widetilde{\kappa} = \kappa/E_0$, and $\widetilde{\eta} = \eta E_0 t_0$. An edge stiffness normalizes in the same way as μ. Tildes are suppressed in the computations.

The physical assumptions are fixed site coordinates, a Euclidean amplitude metric, real internal coordinates with quadratic restoring energy, positive exponential stiffness, and constant scalar mobilities with the stated reciprocal coupling. They define a viable finite model. They do not establish a particular material realization, a thermal bath, detailed balance of an underlying stochastic process or a measured fluctuation–dissipation relation.

Theorem 2.1 (Global evolution and dissipation)**.** *For every initial state (z_0, m_0), equations (5)–(6) have a unique smooth solution for all $t \geq 0$. For all such times,*

$$K(m) \geq \mu I, \tag{7}$$

$$\frac{dF}{dt} = -\gamma \left\| K(m) z \right\|^2 - \eta \left\| \nabla_m F \right\|^2, \tag{8}$$

$$\|z(t)\| \leq \|z_0\| \, e^{-\gamma \mu t}. \tag{9}$$

If $F_0 = F(z_0, m_0)$ and $R = \sqrt{2F_0/\kappa}$, then $|m(t)| \leq R$ and

$$\|K(m(t))\| \leq M := \mu + e^R \sum_e \|B_e\|. \tag{10}$$

Proof. Every B_e is nonnegative, proving (7). The skew symmetry of J gives

$$(\nabla_q F)^\top J \nabla_q F = 0.$$

The chain rule in (4) now gives (8). Moreover

$$\frac{d}{dt} \|z\|^2 = -2\gamma z^* K(m) z \leq -2\gamma\mu \|z\|^2,$$

which proves (9). The smooth vector field is locally Lipschitz. Its solution remains in the energy sublevel because F decreases. The estimate $F \geq \mu \|z\|^2/2 + \kappa |m|^2/2$ makes that sublevel compact in the finite state space. No finite-time escape is possible, so the local solution extends globally. The memory bound and triangle inequality give (10). Smoothness follows from the smooth vector field. □

Proposition 2.2 (Relaxation of memory)**.** *Let $Z = \|z_0\|$. Each memory coordinate obeys*

$$|m_e(t)| \leq |m_e(0)| e^{-\eta\kappa t} + \frac{\eta}{2} e^R \|b_e\|^2 Z^2 I(t), \tag{11}$$

where

$$I(t) = \begin{cases} \dfrac{e^{-2\gamma\mu t} - e^{-\eta\kappa t}}{\eta\kappa - 2\gamma\mu}, & \eta\kappa \neq 2\gamma\mu, \\ t e^{-\eta\kappa t}, & \eta\kappa = 2\gamma\mu. \end{cases} \tag{12}$$

Consequently $m(t) \to 0$, $z(t) \to 0$ and $K(m(t)) \to K(0)$.

Proof. Variation of constants in (6) gives the exact expression

$$m_e(t) = e^{-\eta\kappa t} m_e(0) - \frac{\eta}{2} \int_0^t e^{-\eta\kappa(t-s)} e^{m_e(s)} |b_e^\top z(s)|^2 \, ds.$$

Use $e^{m_e(s)} \le e^R$ and (9). The remaining convolution is $I(t)$. Its explicit expressions both tend to zero, proving the assertion by continuity of (1). □

Thus the unforced model has one equilibrium, $(0, 0)$, and every trajectory returns to it. Adaptation can modify a transient without producing sustained organization. No assumption of a positive joint Hessian was used in Theorem 2.1; coercivity and positive partial amplitude curvature suffice for this conclusion.

Proposition 2.3 (Collective calibration mode)**.** *If $b_e^\top \mathbf{1} = 0$ for every edge, then*

$$\overline{z}(t) := \frac{1}{n} \mathbf{1}^\top z(t) = \overline{z}(0) e^{-(\gamma + \mathrm{i}\alpha)\mu t}. \tag{13}$$

Proof. $\mathbf{1}^\top K(m) = \mu \mathbf{1}^\top$ at every state. Multiply (5) by $\mathbf{1}^\top / n$ and solve the scalar equation. □

This mode is retained in our numerical preparation. It provides an exact control, but it is insensitive to the adapting edge contrasts. For any conditional history the norm of its amplitude propagator is exactly $e^{-\gamma\mu t}$: the contraction bound is attained on $\mathbf{1}$. A propagator norm alone therefore cannot identify adaptation in this network.

2.2 Instantaneous CSCF realization

At fixed m, the partial amplitude Hessian is K_R, which commutes with J. In complex coordinates the dissipative and coherent generators are

$$K_d(m) = \gamma K(m), \qquad C(m) = \alpha K(m) = h(K_d(m)). \tag{14}$$

On the reachable spectral interval, $h(\lambda) = (\alpha/\gamma)\lambda$. To meet the bounded nondecreasing symbol convention of CSCF, one can take $h(\lambda) = (\alpha/\gamma) \min\{\lambda, \gamma M\}$ on $[0, \infty)$. This fixes the actual functional calculus on the trajectory, is nonzero on its positive spectrum, and vanishes at zero. The extension depends on the declared energy class through M; it is not a cutoff-independent prediction of a unique physical symbol. With a static carrier the original factorization follows immediately. The next section determines its replacement for the evolving carrier.

3 Conditional evolution and time ordering

Fix one realized memory path $m(t)$ on $[0, T]$, and hence a prescribed Hermitian $K(t)$. In this section it is sufficient that K be bounded and piecewise continuous with $K(t) \ge 0$. The adaptive source supplies the stronger smoothness and lower bound μI. Set $c = \gamma + \mathrm{i}\alpha$ and define two-parameter propagators by

$$\partial_t U(t, s) = -cK(t)U(t, s), \qquad U(s, s) = I, \tag{15}$$

$$\partial_t D(t, s) = -\gamma K(t)D(t, s), \qquad D(s, s) = I, \tag{16}$$

$$\partial_t V(t, s) = -\mathrm{i}\alpha K(t)V(t, s), \qquad V(s, s) = I. \tag{17}$$

They obey the evolution-family composition law. Forward U, D are contractions and V is unitary, by differentiating squared vector norms. If $K(t) \ge \mu I$, the first two norms are at most $e^{-\gamma\mu(t-s)}$. Generally they are not one-parameter semigroups or groups, since shifting the initial time changes the intervening history. Write $U(t) = U(t, 0)$ and similarly for D, V.

Theorem 3.1 (Exact interaction picture)**.** *There is an exact factorization*

$$U(t) = V(t)R(t), \qquad \dot{R}(t) = -\gamma V(t)^* K(t) V(t) R(t), \quad R(0) = I. \tag{18}$$

The rotated dissipative carrier remains positive. In general $R \neq D$.

Proof. Set $R = V^*U$. Unitarity and (17) give $\partial_t V^* = \mathrm{i}\alpha V^* K$. Differentiation cancels the reactive terms and leaves $\dot{R} = -\gamma V^* K U = -\gamma V^* K V R$. This proves the identity and positivity follows by unitary congruence. □

At each time $[\gamma K(t), \alpha K(t)] = 0$. This does not remove $[K(t), K(s)]$ at different times. The interaction picture retains that information through the rotating carrier. It gives a constructive attenuation law rather than replacing time ordering by an instantaneous diagonalization.

Theorem 3.2 (Gap-free factorization estimate)**.** *Under the hypotheses above,*

$$\|U(T) - D(T)V(T)\| \leq \gamma|\alpha| \int_0^T \int_0^t \|[K(t), K(s)]\| \, ds \, dt. \tag{19}$$

If K is continuously differentiable, $\|K(t)\| \leq M$ and $\left\|\dot{K}(t)\right\| \leq L$, then the right side is at most $\gamma|\alpha| MLT^3/3$. For $K(t) = K_0 + tA$ it is $\gamma|\alpha| \, \|[A, K_0]\| \, T^3/6$.

Proof. For fixed terminal t, the matrix $K(t)$ is constant in the following integral identity. Differentiating $D(t,s)K(t)D(s,0)$ in s and integrating gives

$$[K(t), D(t)] = -\gamma \int_0^t D(t,s)[K(t), K(s)]D(s,0) \, ds. \tag{20}$$

Let $W(t) = D(t)V(t)$. Direct differentiation with the displayed ordering yields

$$\dot{W} + cK(t)W = \mathrm{i}\alpha[K(t), D(t)]V(t). \tag{21}$$

Since $U(0) - W(0) = 0$, variation of constants in the U equation bounds $\|U(T) - W(T)\|$ by the integral of the norm of the right side. Use contraction of the two D factors and $U(T,t)$, unitarity of V, and (20) to obtain (19).

For the differentiable case,

$$\|[K(t), K(s)]\| = \|[K(t) - K(s), K(s)]\| \leq 2ML(t-s).$$

The double integral of $t - s$ is $T^3/6$. For an affine path the exact commutator is $(t-s)[A, K_0]$, giving the sharper constant. □

The estimate requires no spectral gap and remains valid at degeneracies or crossings. It prices precisely the failure of separate attenuation and phase propagation. Globally commuting histories are sufficient for zero error: all three propagators then equal exponentials of their integrated generators and factor exactly. Equality at a single endpoint is a weaker statement and does not establish pairwise commutation of the entire history.

Instantaneous eigenvectors are optional coordinates, not part of the proof. If a differentiable unitary basis $Q(t)$ diagonalizes $K(t)$, then $u = Q(t)^* z$ obeys

$$\dot{u} = -c\Lambda(t)u - Q(t)^* \dot{Q}(t) u. \tag{22}$$

The connection is skew-Hermitian but generally couples modes. At a crossing a unique smooth eigenvalue-ordered basis need not exist. Working in the fixed physical coordinates avoids that extra assumption while retaining the connection whenever such coordinates are used.

3.1 Two pulses and asymptotic sharpness

Take $K(t) = K_1$ for a duration τ, followed by K_2 for the same duration. The endpoint is $T = 2\tau$, with

$$U = e^{-c\tau K_2}e^{-c\tau K_1}, \quad D = e^{-\gamma\tau K_2}e^{-\gamma\tau K_1}, \quad V = e^{-\mathrm{i}\alpha\tau K_2}e^{-\mathrm{i}\alpha\tau K_1}. \tag{23}$$

Taylor multiplication, retaining the order of all second-degree terms, gives

$$U - DV = \mathrm{i}\gamma\alpha\tau^2[K_2, K_1] + O(\tau^3), \tag{24}$$

$$U - U_{\mathrm{rev}} = c^2\tau^2[K_2, K_1] + O(\tau^3), \tag{25}$$

where $U_{\mathrm{rev}} = e^{-c\tau K_1}e^{-c\tau K_2}$. The remainder is in operator norm for fixed finite matrices and coefficients as $\tau \downarrow 0$. To see (24), the ordered mixed term in U has coefficient $c^2K_2K_1$; subtracting the mixed terms of DV leaves $\mathrm{i}\gamma\alpha(K_2K_1 - K_1K_2)$. Subtracting the reversed product directly gives (25). Equation (19) here is

$$\|U - DV\| \le \gamma|\alpha|\tau^2 \, \|[K_2, K_1]\| \, . \tag{26}$$

For a nonzero commutator its leading constant is attained asymptotically. Pulse reversal preserves the two pulse spectra and $\int_0^{2\tau} K(t)\,dt$, but changes the response. Consequently neither quantity determines U in general. The naive integrated-carrier exponential also differs at second order, by $(c^2\tau^2/2)[K_2, K_1] + O(\tau^3)$.

3.2 A moving but commuting control

For the three-node path let $b_1 = (1, -1, 0)^\top$, $b_2 = (0, 1, -1)^\top$, and $w_e(t) = e^{m_e(t)}$. Then

$$[K(t), K(s)] = [w_1(t)w_2(s) - w_2(t)w_1(s)][B_1, B_2], \tag{27}$$

and $\|[B_1, B_2]\| = \sqrt{3}$. This norm follows by multiplying the two rank-one edge matrices; the resulting real skew matrix has singular values $\sqrt{3}, \sqrt{3}, 0$.

Reflection swaps nodes one and three and swaps the two memories. Equations (5)–(6) are equivariant under that reflection. Uniqueness therefore preserves $z_1 = z_3$ and $m_1 = m_2$ from symmetric initial data. In this sector

$$K(t) = \mu I + w(t)(B_1 + B_2), \tag{28}$$

so all history commutators vanish even if w changes substantially. This is a source-generated control: carrier motion alone does not destroy factorization. For the unrestricted path, a constant ratio w_1/w_2 is likewise sufficient for commutation. The asymmetric calculation in Section 6 contrasts these cases without modifying the mobility law.

4 Full feedback, memory and changing coordinates

The conditional equation treats $m(t)$ as prescribed. A perturbation of the physical source need not do so. Along a source trajectory define the $2n \times p$ matrix $B(t)$ and the $p \times p$ matrix $H_m(t)$ by

$$B_e^{\mathrm{col}} = (\partial_{m_e} K_R)q, \qquad H_m = \kappa I + \mathrm{diag}\left(\frac{1}{2}e^{m_e}|b_e^\top z|^2\right). \tag{29}$$

The notation B_e^{col} denotes a column of B, as distinct from the edge matrix $B_e = b_e b_e^\top$. The complete real Hessian is

$$\mathcal{H}(t) = \begin{pmatrix} K_R & B \\ B^\top & H_m \end{pmatrix}. \tag{30}$$

Although its diagonal blocks are positive, $\mathcal{H}$ need not be nonnegative.

Proposition 4.1 (Complete tangent and exact memory)**.** *The perturbation* $(\xi, \nu) = (\delta q, \delta m)$ *satisfies*

$$\dot{\xi} = -GK_R\xi - GB\nu, \tag{31}$$

$$\dot{\nu} = -\eta B^\top \xi - \eta H_m \nu. \tag{32}$$

Let $R_m(t,s)$ *solve* $\partial_t R_m(t,s) = -\eta H_m(t) R_m(t,s)$ *with* $R_m(s,s) = I$*. Then*

$$\begin{aligned}\dot{\xi}(t) = & -GK_R(t)\xi(t) - GB(t)R_m(t,0)\nu(0) \\ & + \eta \int_0^t GB(t)R_m(t,s)B(s)^\top \xi(s)\, ds.\end{aligned} \tag{33}$$

Proof. Differentiate (4). Constancy of the mobilities means that only the Hessian blocks appear, giving (31)–(32). Variation of constants yields

$$\nu(t) = R_m(t,0)\nu(0) - \eta \int_0^t R_m(t,s)B(s)^\top \xi(s)\, ds.$$

Substitution gives (33) with its positive kernel sign and negative initial-memory term. No adiabatic or Markov approximation is used. □

Here H_m is diagonal, so R_m can also be written as the exponential of its time integral, and $\|R_m(t,s)\| \le e^{-\eta\kappa(t-s)}$. The product with $GB(t)$ is still generally neither symmetric nor a scalar function of the amplitude carrier. The time dependence prevents replacing this kernel by a stationary convolution without further assumptions.

If memory is clamped at the same realized path during a small amplitude probe, ν is constrained to zero by the preparation apparatus. Its amplitude response is precisely the realification of $U(t,s)$. If instead $\nu(0) = 0$ but memory is free to respond, (32) immediately generates ν through $B^\top\xi$. Zero initial memory perturbation does not eliminate the kernel. The two responses coincide under appropriate decoupling, for example $B = 0$ on the trajectory, but they are different observables in general. A clamp is an additional resource whose effects must be controlled when comparing the equations with hardware.

4.1 Exact transient expansion despite partial positivity

Take a scalar complex amplitude, one real memory, $\mu = 2/5$, $\kappa = 1$ and $m = 0$. At $z = 3$ real, the $(\Re z, m)$ Hessian block is

$$\begin{pmatrix} 7/5 & 3 \\ 3 & 11/2 \end{pmatrix}, \qquad \det = -13/10. \tag{34}$$

The imaginary-amplitude diagonal is also $7/5$ and has zero memory cross term at this state. For the real perturbation $v = (\delta\Re z, \delta\Im z, \delta m) = (1, 0, -1/2)$,

$$v^\top \mathcal{H} v = -9/40, \qquad \frac{d}{dt}(|\xi|^2 + |\nu|^2)\Big|_{t=0} = 9/20 \tag{35}$$

when $\gamma = \eta = 1$, for every α. Indeed the reactive contribution to the norm derivative vanishes at this particular real perturbation, while the dissipative contribution is $-2v^\top\mathcal{H}v$. Thus positive partial amplitude curvature and conditional amplitude contraction do not imply contraction of the full feedback tangent. This does not contradict energy decrease or global relaxation of the source; the tangent measures sensitivity between trajectories at a nonstationary state.

Even positive joint curvature need not restore the original complex-alignment hypothesis. At $z = 1/10$ real and $m = 0$,

$$\mathcal{H} = \begin{pmatrix} 7/5 & 0 & 1/10 \\ 0 & 7/5 & 0 \\ 1/10 & 0 & 201/200 \end{pmatrix} > 0. \tag{36}$$

Its commutator with $\mathrm{diag}(J, 0)$ has nonzero entries of magnitude $1/10$. In addition, $\mathrm{diag}(J, 0)$ is a degenerate skew structure on amplitudes plus real memory, not a complex structure on the complete state. The aligned amplitude subclass therefore does not automatically extend to the joint Hessian. The rational calculations behind both examples are included in the verification package.

4.2 The connection for a changing mobility metric

The adaptive source above has a fixed metric. A separate prescribed-metric calculation identifies the additional term when the metric changes. Let $M(t) > 0$ and $H(t) = H(t)^*$ be complex matrices, with M continuously differentiable and H continuous, and consider

$$\dot{x} = -cM(t)H(t)x. \tag{37}$$

Set $S(t) = M(t)^{1/2}$ and $y = S^{-1}x$. Differentiating $x = Sy$ gives the exact equation

$$\dot{y} = -c\underbrace{SHS}_{K_y(t)}y - \underbrace{S^{-1}\dot{S}}_{A_{\mathrm{conn}}(t)}\, y. \tag{38}$$

If $H \geq 0$, then $K_y \geq 0$, but A_{conn} is generally not skew-Hermitian or a function of K_y. In particular,

$$\frac{d}{dt}\,\|y\|^2 = -2\gamma y^* K_y y - y^*(A_{\mathrm{conn}} + A_{\mathrm{conn}}^*)y. \tag{39}$$

Neither positivity of K_y nor static whitening removes the second term. A state-dependent metric along a nonlinear source may also contribute derivative terms to its tangent equation; (38) is a prescribed smooth-path identity, not the complete tangent formula for every such source.

For an explicit diagonal fixture take $M = \mathrm{diag}(e^{2rt}, e^{-2rt})$, $H = \mathrm{diag}(1, 2)$, $r = 1$, $\gamma = 0.2$, $\alpha = 0.4$ and $x(0) = (0, 1)^\top$. Then

$$x_2(t) = \exp[-c(1 - e^{-2rt})/r], \qquad y_2(t) = e^{rt}x_2(t). \tag{40}$$

At $t = 0.1$ the source norm is 0.964395 and the whitened norm is 1.065822. Omitting the connection predicts $y_2 = x_2$ and changes the result by 0.101426. This is growth in a moving coordinate norm, not evidence of physical active gain. The original fixed-metric network requires no such unpriced term.

4.3 Why the autonomous closure certificate changes

For a fixed selfadjoint $K \geq 0$ and an isometry $\mathcal{I}$ onto a retained subspace, the CSCF closure certificate uses the positive Gram defect

$$\mathcal{I}^* e^{-2tK}\mathcal{I} - (\mathcal{I}^* e^{-tK}\mathcal{I})^2 = (Qe^{-tK}\mathcal{I})^*(Qe^{-tK}\mathcal{I}), \quad Q = I - \mathcal{I}\mathcal{I}^*.$$

This relies on selfadjoint semigroup multiplication. For a nonautonomous D, the correct insertion identity is instead

$$\begin{aligned} &\mathcal{A}(t, r) - \mathcal{A}(t, s)\mathcal{A}(s, r) \\ &\qquad = \mathcal{I}^* D(t, s)QD(s, r)\mathcal{I}, \qquad \mathcal{A}(t, s) = \mathcal{I}^* D(t, s)\mathcal{I}. \end{aligned} \tag{41}$$

It follows by inserting $I = \mathcal{I}\mathcal{I}^* + Q$ into $D(t,r) = D(t,s)D(s,r)$. The right side is not generally a Gram matrix.

Two positive-pulse fixtures make the distinction decisive. In one dimension, let $\gamma = 1$, $K = 1$ on $[0,1]$ and $K = 2$ on $(1,2]$. Then $D(2,0) - D(1,0)^2 = e^{-3} - e^{-2} < 0$, even though no hidden sector exists. Separately, let

$$K_1 = \begin{pmatrix} 2 & 1 \\ 1 & 2 \end{pmatrix}, \quad K_2 = \begin{pmatrix} 2 & -1 \\ -1 & 2 \end{pmatrix}, \quad P = \mathrm{diag}(1,0). \tag{42}$$

These positive matrices commute and sum to $4I$. Unit-duration pulses give $D(2,0) = e^{-4}I$, hence zero endpoint leakage $(I-P)D(2,0)P$, while $[P, K_1] \neq 0$. Endpoint invariance therefore does not establish invariance at every intermediate time, even for this commuting history. The autonomous certificate remains valid in its original hypotheses; these examples rule out its unchanged transfer to general evolving histories.

5 A calibrated test of linked operator response

The conditional law is observationally stronger than a comparison of decay-rate and frequency lists. Write $\dot{z} = -A(t)z$ in fixed calibrated coordinates and define Hermitian matrices

$$H_A = \frac{A + A^*}{2}, \qquad C_A = \frac{A - A^*}{2\mathrm{i}}. \tag{43}$$

For the linked source along a common memory history,

$$H_A = \gamma K, \qquad C_A = \alpha K = r H_A, \quad r = \alpha/\gamma. \tag{44}$$

The relation includes common eigenvectors and scalar action on every degenerate carrier eigenspace. It is stronger than commutation, and stronger than matching the two eigenvalue multisets up to scale.

As a restricted alternative, fix a unitary S and replay the same carrier history with

$$A_{\mathrm{alt}}(t) = \gamma K(t) + \mathrm{i}\alpha S K(t) S^*. \tag{45}$$

Its Hermitian part remains γK, so it is accretive and forward contractive. Its coherent eigenvalue multiset equals that of αK, but its coherent eigenvectors are rotated. Its exact linked-law residual is $\alpha(SKS^* - K)$, which is nonzero whenever S fails to preserve K. Such an alternative is not automatically another solution of the original unforced memory law with the same history. The comparison assumes recorded-history replay or clamping for both generators. It isolates a conditional operator claim under that resource contract.

5.1 Short-time reconstruction and a controlled remainder

Let $\Phi(t+u,t)$ solve $\partial_u \Phi = -A(t+u)\Phi$, $\Phi(t,t) = I$. For known t define

$$L_h = \frac{I - \Phi(t+h,t)}{h}, \qquad \widehat{A}_h = 2L_{h/2} - L_h. \tag{46}$$

This avoids selecting a matrix-logarithm branch. Its error is controlled in the same operator norm used for the linked residual.

Theorem 5.1 (Bias, operator noise and calibration)**.** *Assume A is C^2 on $[t, t+h]$, its Hermitian part is nonnegative, and*

$$\|A\| \le a_0, \qquad \|A'\| \le a_1, \qquad \|A''\| \le a_2$$

throughout that interval. Put $B_3 = a_2 + 3a_0a_1 + a_0^3$. *The noiseless estimate obeys*

$$\left\|\widehat{A}_h - A(t)\right\| \le h^2 B_3/4. \tag{47}$$

If each reconstructed propagator at h *and* $h/2$ *has error at most* ε *in operator norm, the measured estimate* $\widetilde{A}_h$ *obeys*

$$\left\|\widetilde{A}_h - A(t)\right\| \le e_h := h^2 B_3/4 + 5\varepsilon/h. \tag{48}$$

Let $\widetilde{H}, \widetilde{C}$ *be its Hermitian parts. If the linked model holds and an independent calibration gives* $|r - r_0| \le \delta_r$, *then*

$$\left\|\widetilde{C} - r_0\widetilde{H}\right\| \le (1 + |r_0|)e_h + \delta_r(\left\|\widetilde{H}\right\| + e_h). \tag{49}$$

Proof. Differentiating the propagator in u gives

$$\Phi'' = (-A' + A^2)\Phi, \tag{50}$$

$$\Phi''' = (-A'' + 2A'A + AA' - A^3)\Phi. \tag{51}$$

Accretivity makes $\|\Phi\| \le 1$, so $\|\Phi'''\| \le B_3$. Taylor's formula with integral remainder gives a quadratic expansion of Φ with remainder at most $u^3B_3/6$. Consequently $L_u = A(t) - u\Phi''(0)/2 + E_u$, where $\|E_u\| \le u^2B_3/6$. In $2L_{h/2} - L_h$ the linear bias cancels, while $2\left\|E_{h/2}\right\| + \|E_h\| \le h^2B_3/4$.

The measured estimate weights the two propagator errors by $-4/h$ and $1/h$, respectively. Their total norm is at most $5\varepsilon/h$, proving (48). Hermitian and anti-Hermitian extraction each have norm at most one, so $\left\|\widetilde{H} - H_A\right\|, \left\|\widetilde{C} - C_A\right\| \le e_h$. Finally

$$\widetilde{C} - r_0\widetilde{H} = (\widetilde{C} - C_A) - r_0(\widetilde{H} - H_A) + (r - r_0)H_A.$$

Use $\|H_A\| \le \left\|\widetilde{H}\right\| + e_h$ to obtain (49). □

The response theorem is conditional on known derivative and measurement bounds. The adaptive trajectory is smooth, but that fact alone does not supply a numerical apparatus error certificate. For fixed B_3 and ε, minimizing the displayed bias–noise upper bound gives $h^3 = 10\varepsilon/B_3$ when this duration remains inside the calibrated smoothness window. If B_3 itself varies with the probe duration or other errors dominate, that algebraic choice need not be optimal.

For exact ratio calibration, the absolute operator residual has uncertainty at most $b = (1 + |r|)e_h$. The linked model yields a measured residual at most b. An alternative with exact residual lower bound $\Delta > 2b$ yields a measured residual above b, provided the same valid uncertainty bound applies to both hypotheses. More generally, let b_L bound the linked model's measured residual and let b_A bound reconstruction error in the alternative's residual, both evaluated with the same nominal ratio r_0. An alternative lower bound $\Delta_0 > b_L + b_A$ for the exact nominal residual then separates the two error bands. Calibration uncertainty enters b_L through (49), and must enter Δ_0 if the alternative's predicted residual depends on the uncertain ratio. Different hypotheses may require different derivative bounds; a bound proved only for the linked model cannot certify the alternative. These are deterministic separation conditions, not significance levels.

5.2 Preparation, metric and access

Reconstructing a complete complex $n \times n$ propagator requires n linearly independent complex preparation columns and phase-sensitive outputs in the same coordinate convention. In a physical small-signal implementation these are small probes about a prepared baseline, with a controlled linearization remainder. Preparation conditioning, detector gain and phase, baseline subtraction and any memory drift must enter the propagator-error bound. Repeated columns must encounter an identical prescribed history, which can require reinitialization, active clamping or faithful replay. A recorded history alone does not guarantee that the apparatus can impose it.

Time and the amplitude metric are substantive calibration data. A general nonunitary coordinate change alters adjoints and hence the two Hermitian parts in (43); a moving metric adds the connection in (38). Testing proportionality in an uncalibrated gain basis is a different assertion. The ratio r_0 should be obtained independently of the tested response. Fitting r by least squares to the same matrices tests only whether *some* proportionality fits; it does not verify an independently predicted mobility ratio. We report such fitted values only as diagnostics alongside the residual using the stipulated $r = 2$.

The numerical study below uses a relative Frobenius residual for convenient reporting. Theorem 5.1 uses an absolute operator norm. In dimension n, operator errors bounded by e_h imply Frobenius errors at most $\sqrt{n}e_h$, so a conservative absolute Frobenius threshold follows by that conversion. Dividing by a small estimated $\|C_A\|_F$ introduces another conditioning issue. No numerical relative residual alone is advertised as an instrument-certified realization of the theorem.

The test distinguishes the nominated linked law from restricted alternatives such as (45). It does not identify every microscopic source representation. Models with identical complete allowed response records remain indistinguishable by those records. This target-relative limit is part of the source-to-readout contract, rather than a defect repaired by collecting more of the same pooled eigenvalue statistic.

6 Executed finite calculations

All calculations in this section are synthetic evaluations of the declared equations. Their parameters, deterministic preparations and acceptance criteria are supplied as machine-readable specifications. No random seed is needed because no random sampling is used. The pulse, feedback, response and symmetry criteria were specified before their respective numerical outcomes; the short-time response probes use a trajectory that had already been inspected. They are tests of equations and observables, not untouched empirical holdouts.

6.1 Feedback trajectory and independent formulation

The three-node path of (27) is used with

$$\mu = 0.4, \quad \kappa = 1, \quad \gamma = 0.6, \quad \alpha = 1.2, \quad \eta = 0.8, \quad T = 2, \tag{52}$$

$$z_0 = (1 + 0.2\mathrm{i}, -0.4 + 0.7\mathrm{i}, 0.2 - 0.3\mathrm{i})^\top, \qquad m_0 = (0.15, -0.1)^\top. \tag{53}$$

DOP853 integrates the source and accumulated dissipation with relative tolerance 10^{-11} and absolute tolerance 10^{-13}, retaining 401 equally spaced samples. A separate classical RK4 computation uses 4,000 fixed steps and a real-coordinate gradient evaluation assembled edge by edge, without calling the complex source right-hand side. Its endpoint comparison covers the eight source coordinates and the accumulated loss. This is an independent numerical formulation of the same model, not independent physical evidence.

The full 8×8 tangent and conditional 6×6 real amplitude propagator are integrated along the same trajectory. The test direction is a unit perturbation of the first real amplitude, with zero initial memory perturbation. Nonlinear central differences with perturbation 10^{-5} check the tangent. Separately integrated complex U, D, V, R verify the interaction picture and measure the error of the static factorization. Table 1 records the results directly from the generated output.

Quantity	Value
Initial energy	2.279×10^{0}
Final energy	4.157×10^{-2}
DOP853 energy-balance residual	1.046×10^{-11}
RK4 energy-balance residual	1.076×10^{-12}
Independent endpoint maximum error	9.766×10^{-13}
Norm-bound maximum excess	0
Full versus clamped response difference	2.379×10^{-2}
Central-difference tangent error	2.947×10^{-11}
Static factorization error	7.322×10^{-3}
Interaction-picture residual	1.236×10^{-12}
Coherent unitarity defect	4.706×10^{-12}

Table 1: Computed feedback and propagation checks in normalized units. Scalar residuals use the definitions and norms stated in the text; they are floating evaluations, not interval enclosures.

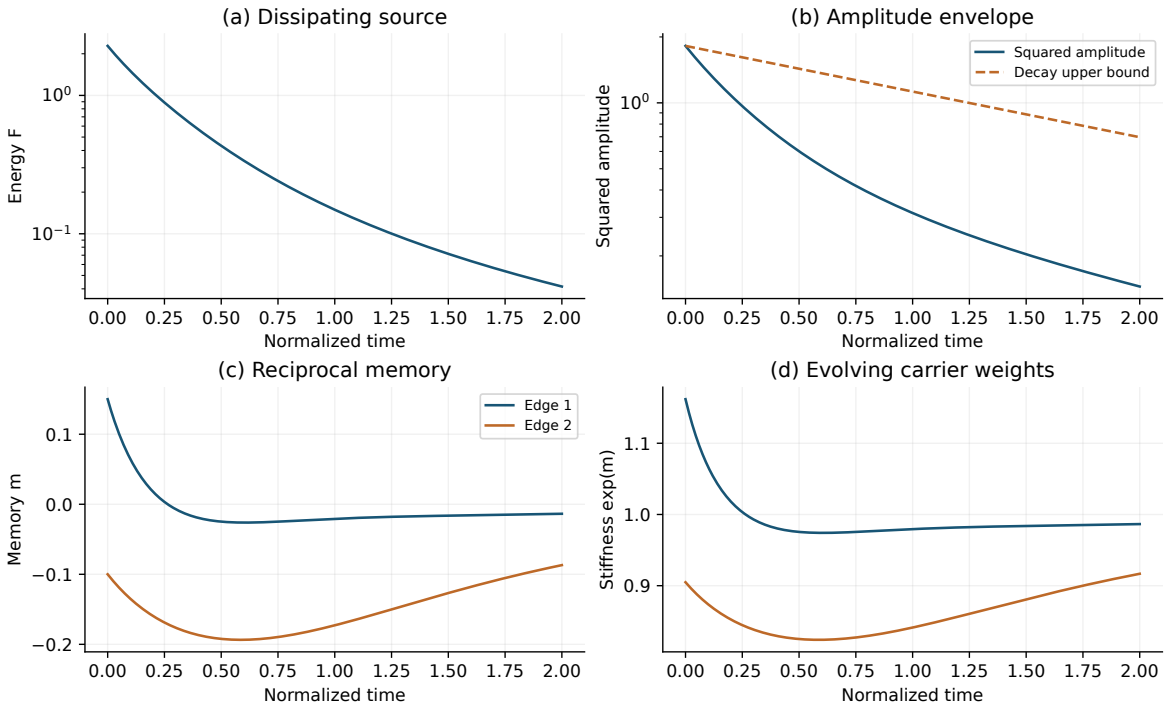


Figure 1: The self-consistent asymmetric trajectory. Energy and squared amplitude decrease, while the two edge memories and stiffnesses evolve differently. The amplitude envelope is the theorem's upper bound, not a fitted decay curve. All quantities use the normalized units of Section 2.

The full versus clamped response difference is about 0.02379, whereas the central-difference tangent error is about 2.95×10^{-11}. Thus the feedback distinction is resolved on this fixture

independently of the conditional factorization error. The collective-mode error is 2.83×10^{-16} at the saved samples. The computed norm of U agrees with $e^{-0.48}$, as Proposition 2.3 predicts, and contains little information about the adapting contrasts.

6.2 Pulse ordering and the symmetric control

The pulse test uses

$$K_1 = \mathrm{diag}(1, 2), \qquad K_2 = \begin{pmatrix} 2 & 1 \\ 1 & 2 \end{pmatrix}, \qquad \gamma = 0.7, \quad \alpha = 1.1. \tag{54}$$

Both matrices are positive and $\|[K_2, K_1]\| = 1$. Matrix exponentials are compared with an independent closed-form 2×2 formula. For a matrix X, set $N = X - (\mathrm{tr}\, X)I/2$ and $d^2 = -\det N$. The identity $N^2 = d^2 I$ gives

$$e^X = e^{\mathrm{tr}\, X/2} \left(\cosh d\, I + \frac{\sinh d}{d} N \right), \tag{55}$$

with the continuous value at $d = 0$. The maximum difference from the matrix-exponential implementation is 3.34×10^{-16} over the specified pulses. Table 2 and Figure 2 show the quadratic factorization error and its approach to the leading commutator coefficient. The bound uses each pulse duration τ, not total duration 2τ.

τ	$\|U - DV\|$	Bound	Leading discrepancy
0.04	1.148×10^{-3}	1.232×10^{-3}	0.19671
0.02	2.974×10^{-4}	3.080×10^{-4}	0.10122
0.01	7.566×10^{-5}	7.700×10^{-5}	0.05134
0.005	1.908×10^{-5}	1.925×10^{-5}	0.02585

Table 2: Two-pulse propagation. The last column is the relative discrepancy of the scaled matrix in equation (24) from its leading commutator.

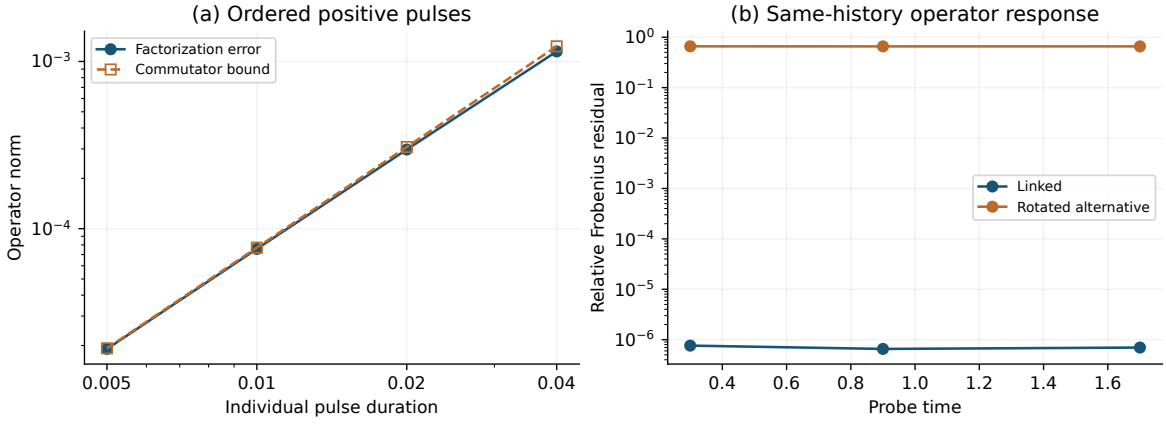


Figure 2: Left: two-pulse factorization error and analytic commutator upper bound versus individual pulse duration. Right: short-time response residual $\left\|\widetilde{C} - 2\widetilde{H}\right\|_F / \left\|\widetilde{C}\right\|_F$ on the recorded adaptive path, for the linked law and the coherent-eigenvector-rotated alternative. The probes preserve the same memory history. Lines connect evaluated values and carry no statistical uncertainty interpretation.

For the symmetric source control, replace z_0 by $(1+0.2\mathrm{i}, -0.4+0.7\mathrm{i}, 1+0.2\mathrm{i})^\top$ and m_0 by $(0.15, 0.15)^\top$, retaining the same coefficients and duration. The maximum memory displacement is 0.202353, while $m_1 - m_2$ remains numerically zero. The factorization residual is 4.34×10^{-13}, compared with 0.007322 for the asymmetric trajectory. A trapezoidal evaluation of the asymmetric commutator integral gives 0.0903793. This last value is an approximation to the bound's integral, not a certified quadrature upper enclosure; the universal assertion is Theorem 3.2.

6.3 Response reconstruction and exact fixtures

The response test reconstructs (46) at times $0.3, 0.9, 1.7$ using $h = 5 \times 10^{-4}$. A cubic spline through the 401 saved memory samples defines the replayed path, and DOP853 uses relative tolerance 10^{-12} and absolute tolerance 10^{-14} for the short propagators. The linked and alternative tests both use that same interpolated path. The distinction between the interpolated path and an imposed physical trajectory belongs to an experiment's drift and reconstruction budget.

For the alternative use the cyclic permutation

$$S = \begin{pmatrix} 0 & 1 & 0 \\ 0 & 0 & 1 \\ 1 & 0 & 0 \end{pmatrix}. \tag{56}$$

Table 3 reports residuals with the stipulated $r = 2$ and diagnostic fitted ratios. Linked relative residuals are below 8×10^{-7}, while the alternative residuals exceed 0.65, despite identical instantaneous coherent eigenvalue multisets. The frozen criteria were respectively 10^{-4} and 0.01. No apparatus noise is inferred from the integration tolerances.

Time	Model	Relative residual	Fitted ratio
0.3	Linked	7.630×10^{-7}	1.9999986
0.3	Rotated	6.590×10^{-1}	1.5656839
0.9	Linked	6.558×10^{-7}	1.9999988
0.9	Rotated	6.572×10^{-1}	1.5681140
1.7	Linked	6.982×10^{-7}	1.9999987
1.7	Rotated	6.578×10^{-1}	1.5672790

Table 3: Same-history response reconstruction. Residuals use the independently stipulated model ratio $r = 2$; the fitted ratio is a diagnostic from the same response.

Separate diagonal exact-propagator fixtures check the extrapolation remainder and the $5\varepsilon/h$ noise amplification. They use $A(t) = c\,\mathrm{diag}(1+t, 2+t/2)$ with $\gamma = 0.7$, $\alpha = 1.1$, durations $0.04, 0.02, 0.01$ and imposed operator perturbations of size 10^{-10}. The closed scalar exponentials provide an independent reference. Numerical inequalities include a 10^{-12} floating allowance; near-equality in the constructed worst-case noise direction is not a directed arithmetic certificate. Exact rational arithmetic checks (34)–(35), joint-Hessian positivity at small amplitude, and its failed reactive alignment. Integer matrix identities and elementary exponential evaluation check the nonautonomous closure fixtures. The prescribed-metric test evaluates (40) directly.

6.4 Public verification and evidence classes

The public package contains the seven scientific scripts, their specifications, saved outputs, figure and table generator, dependencies, provenance, hashes and a runner that writes only

to a fresh output directory. It is used alongside this PDF; the editable manuscript source is distributed separately. Cryptographic checks preserve the reference files, and exact checks retain discrete results, labels, table structure and acceptance definitions. Scientific quantities and trajectory arrays are compared to the reference run with declared numerical tolerances. Small solver and finite-difference residuals are checked against their scientific ceilings rather than required to reproduce identical diagnostic digits.

The tables and reported floating diagnostics refer to the retained reference run using Python 3.12.14, NumPy 2.3.5 and SciPy 1.18.1. Regenerated table values must match their own underlying output to the stated printing precision, while the underlying quantities must pass the separate scientific checks. Text line endings are normalized. Thus an acceptable change in a tiny tangent diagnostic does not rewrite the published reference table or cause a false reproducibility failure. Targeted regressions accept line-ending and admissible diagnostic changes, and reject changed scientific results, labels, structure or acceptance conditions.

Analytic proofs establish the universal finite-dimensional statements under their hypotheses. Rational fixtures verify nominated exact examples. DOP853, RK4 and closed-form matrix computations provide distinct numerical checks. Running the same scripts again establishes reproducibility within the recorded environment. These evidence classes do not substitute for physical implementation, empirical validation or full interval certification. The package excludes the unrelated radial, image and Kerr data because no new result here depends on repeating those campaigns.

7 Consequences and focused extensions

The finite adaptive source resolves a specific extension problem left by the fixed-carrier CSCF construction. One energy supplies a self-consistent carrier and reciprocal feedback. The instantaneous amplitude law remains a linked functional-calculus pair, with the mobility ratio fixing its coherent symbol on the reachable spectrum. Contraction and unitary conditional evolution survive, while one-parameter stationarity and simple global factorization generally do not. The exact interaction picture and the commutator estimate replace the discarded static identity with controlled statements.

The feedback calculation also identifies which source distinctions an observation must retain. The amplitude record alone does not determine its own velocity across all source states. At the linearized level this information loss appears as the initial-memory term and causal kernel. A conditional history and a free feedback perturbation are therefore different experiments. This gives substantive content to the Shadow source-to-readout architecture: the source state, projection, failed descent and sufficient retained history are all explicit. No inference about inaccessible source variables is made solely from spectral recurrence.

The response test moves the physical question beyond parallel eigenvalue fits. A calibrated relation $C_A = rH_A$ predicts common eigenspaces and behavior inside degenerate blocks. The rotated alternative preserves coherent eigenvalues but changes this operator relation. Phase-sensitive probes along a common memory history discriminate that alternative under the stated access and error conditions. The theorem specifies the bias, noise and calibration costs of such a comparison, while the numerical examples establish its operation on the chosen finite model.

7.1 Physical implementation and driven organization

The strongest next implementation step is a prepared three-node network with independently calibrated dissipative and reactive mobilities, known amplitude metric and phase-sensitive outputs. A paired protocol should compare a repeated clamped or replayed memory history with an unclamped feedback kick. The first tests the conditional relation; the second tests

the tangent kernel and its memory backreaction. The alternative law, initialization, probe durations, drift and detector bounds should be fixed before outcomes are examined. The current numerical contrast supplies candidate observables and scales, not hardware feasibility or a device-noise estimate.

The unforced source relaxes to $(0, 0)$. Persistent nonzero amplitudes or memory require a drive and an energy budget. For example, adding a declared amplitude force $f(t)$ changes the balance by the supplied power $\Re[(Kz)^* f]$. Existence of driven attractors, their stability and their response law would then be new questions. The transient adaptation proved here does not establish them.

7.2 Continuum domains and renormalization

The finite proofs avoid unbounded-operator domain questions. A continuum realization must supply a closed energy form, boundary conditions, a well-posed nonlinear source, and evolution-family hypotheses compatible with a time-dependent domain or common form domain. The finite commutator bound cannot be transferred merely by substituting an unbounded differential expression: bounded commutators or controlled graph estimates and their integral convergence would be needed. Eigenvalue crossings alone are not the obstacle addressed by those requirements.

Similarly, instantaneous finite functional calculus does not define an infinite-dimensional determinant budget for an evolving carrier. A cutoff limit would require trace-ideal or another explicitly stated determinant convention, together with its counterterms and convergence estimates. Renormalization, continuum universality and cross-domain microscopic identification remain distinct extensions. None is used as a premise of the results proved here.

8 Conclusion

A self-consistently evolving positive carrier supports linked instantaneous attenuation and phase when its energy, metric and reactive/dissipative mobilities have the stated alignment. Time ordering modifies the finite response through cross-time carrier commutators. Reciprocal memory modifies the full feedback sensitivity through retained initial-state and causal terms. Calibrated operator probes can test the linked law against eigenvalue-preserving alternatives, provided their preparation histories and error budgets are controlled. Together these results supply an adaptive CSCF realization with explicit mathematical and observational return conditions.

References

[1] Jeremy Rodgers. The canonical spectral-curvature field: A unified operator origin for coherence, dissipation, and spectral budgets. Zenodo, 2026. URL https://doi.org/10.5281/zenodo.23899458. Preprint, issued 3 November.

[2] Igor S. Aranson and Lorenz Kramer. The world of the complex Ginzburg–Landau equation. *Reviews of Modern Physics*, 74:99–143, 2002. doi: 10.1103/RevModPhys.74.99. URL https://arxiv.org/abs/cond-mat/0106115.

[3] Tosio Kato. Integration of the equation of evolution in a Banach space. *Journal of the Mathematical Society of Japan*, 5(2):208–234, 1953. doi: 10.2969/jmsj/00520208. URL https://www.jstage.jst.go.jp/article/jmath1948/5/2/5_2_208/_article/-char/en.

[4] S. Blanes, F. Casas, J. A. Oteo, and J. Ros. The Magnus expansion and some of its applications. *Physics Reports*, 470:151–238, 2009. doi: 10.1016/j.physrep.2008.11.001. URL https://arxiv.org/abs/0810.5488.

[5] Jeremy Rodgers. Observable quotients and exact projected dynamics: Closure, memory, minimal dynamical completion, and effective field operators. Zenodo, 2026. URL https://doi.org/10.5281/zenodo.21371251. Preprint, issued 15 July.

[6] Jeremy Rodgers. From source structure to spectral profiles: Generation mechanisms and observable readouts in the canonical spectral-curvature framework. Zenodo, 2026. URL https://doi.org/10.5281/zenodo.23912447. Preprint, issued 3 November.

[7] Jeremy Rodgers. Cross-domain spectral ratio structure: Refined recurrence, robustness and diagnostic limits. Zenodo, 2026. URL https://doi.org/10.5281/zenodo.23888292. Preprint, issued 2 November.

[8] Jeremy Rodgers. Source readout non-equivalence: Descent and equivariant reconstruction obstructions. Zenodo, 2026. URL https://doi.org/10.5281/zenodo.21369967. Preprint, issued 15 July.